Science Bulletin 70 (2025) 4142–4145

Contents lists available at ScienceDirect

Science Bulletin

journal homepage: www.elsevier.com/locate/scib

Short Communication

Dynamic ventilation functional MRI of the lung with sub-millimeter spatial resolution and millisecond temporal resolution

Hongchuang Li [a,b,1], Haidong Li [a,b,1], Li Fan [c,1], Ming Zhang [a,b], Xiaoling Liu [a,b], Xiuchao Zhao [a,b], Yeqing Han [a,b], Yang Jin [e], Louis-S. Bouchard [f], Shiyuan Liu [c], Xin Zhou [a,b,d,*]

[a] State Key Laboratory of Magnetic Resonance Spectroscopy and Imaging, National Center for Magnetic Resonance in Wuhan, Wuhan Institute of Physics and Mathematics, Innovation Academy for Precision Measurement Science and Technology, Chinese Academy of Sciences, Wuhan 430071, China
[b] University of Chinese Academy of Sciences, Beijing 100049, China
[c] Department of Radiology, Second Affiliated Hospital of Naval Medical University, Shanghai 200003, China
[d] Key Laboratory of Biomedical Engineering of Hainan Province, School of Biomedical Engineering, Hainan University, Haikou 570228, China
[e] Department of Respiratory and Critical Care Medicine, Union Hospital, Tongji Medical College, Huazhong University of Science and Technology, Wuhan 430022, China
[f] Departments of Chemistry and Biochemistry, University of California, Los Angeles, CA 90095, USA

ARTICLE INFO

Article history:
Received 25 January 2025
Received in revised form 7 April 2025
Accepted 7 May 2025
Available online 13 May 2025

Pulmonary dynamic ventilation dysfunction is a common feature of various lung diseases, including chronic obstructive pulmonary disease (COPD) [1], cystic fibrosis [2], and asthma [3]. Regional assessment of ventilation dynamics offers substantial potential to enhance diagnostic accuracy and therapeutic monitoring in these conditions. Although current clinical evaluations primarily depend on global pulmonary function tests, emerging imaging modalities such as four-dimensional computed tomography (4D-CT) [4] and phase-resolved functional lung (PREFUL) imaging [5] enable temporal observation of structural and ventilation changes. However, these techniques are fundamentally limited in their ability to visualize time-of-flight (TOF) gas flow patterns within airways and alveolar spaces-critical parameters for the direct assessment of regional gas diffusion efficiency.

Hyperpolarized (HP) ^{129}Xe magnetic resonance imaging (MRI) has emerged as a powerful modality for non-invasive assessment of pulmonary structure and functional dynamics [6] and has received clinical approval in both China and the United States [7]. Several studies employing HP gas MRI, combined with multiple-breath wash-in/wash-out techniques, have investigated lung dynamic ventilation function and ventilation heterogeneity. Additionally, HP gas MRI has been utilized to assess dynamic ventilation function, including delayed ventilation [8], inflation rate [9], and gas flow within the major airways [10].

Continuous image acquisition throughout the respiratory cycle is essential for dynamic ventilation analysis. However, this requirement poses substantial technical challenges due to the inherent mismatch between the short duration of physiological breaths (particularly in preclinical models) and the temporal resolution limitations of conventional MRI acquisition. Although acceleration strategies such as sliding window reconstruction and interleaved spiral imaging can improve temporal sampling, these approaches inevitably compromise signal-to-noise ratio (SNR) and spatial resolution. Compressed sensing (CS) methodologies have advanced human imaging temporal resolutions into the sub-second range [11], but they remain insufficient for detecting subtle pathophysiological changes, particularly in small animal models.

To address these limitations, we present a novel method for high spatiotemporal resolution imaging of pulmonary ventilation dynamics across multiple respiratory cycles by using ^{129}Xe gas MRI (Fig. 1). To overcome the challenge posed by short breath cycles *in vivo*, we employ a combination of multiple-breath ventilation and line-scan acquisition strategies [12]. This approach enables the reconstruction of high-temporal resolution images by synchronizing data from multiple breaths into a single respiratory cycle. Each frame of the dynamic images was captured across separated breath cycles, with only one k-space line acquired per frame during a single breath (Fig. 1a). To eliminate the influence of residual HP ^{129}Xe gas MRI signals from the previous breath, sixteen saturation RF pulses were applied at the onset of ^{129}Xe inspiration in each respiration cycle (Fig. 1b). Additionally, a 7° flip angle RF excitation pulse was used for all the dynamic acquisitions to maintain a relatively high SNR (Fig. 1b). To shorten the scan time, a

* Corresponding author.
E-mail address: xinzhou@wipm.ac.cn (X. Zhou).
[1] These authors contributed equally to this work.

https://doi.org/10.1016/j.scib.2025.05.014
2095-9273/

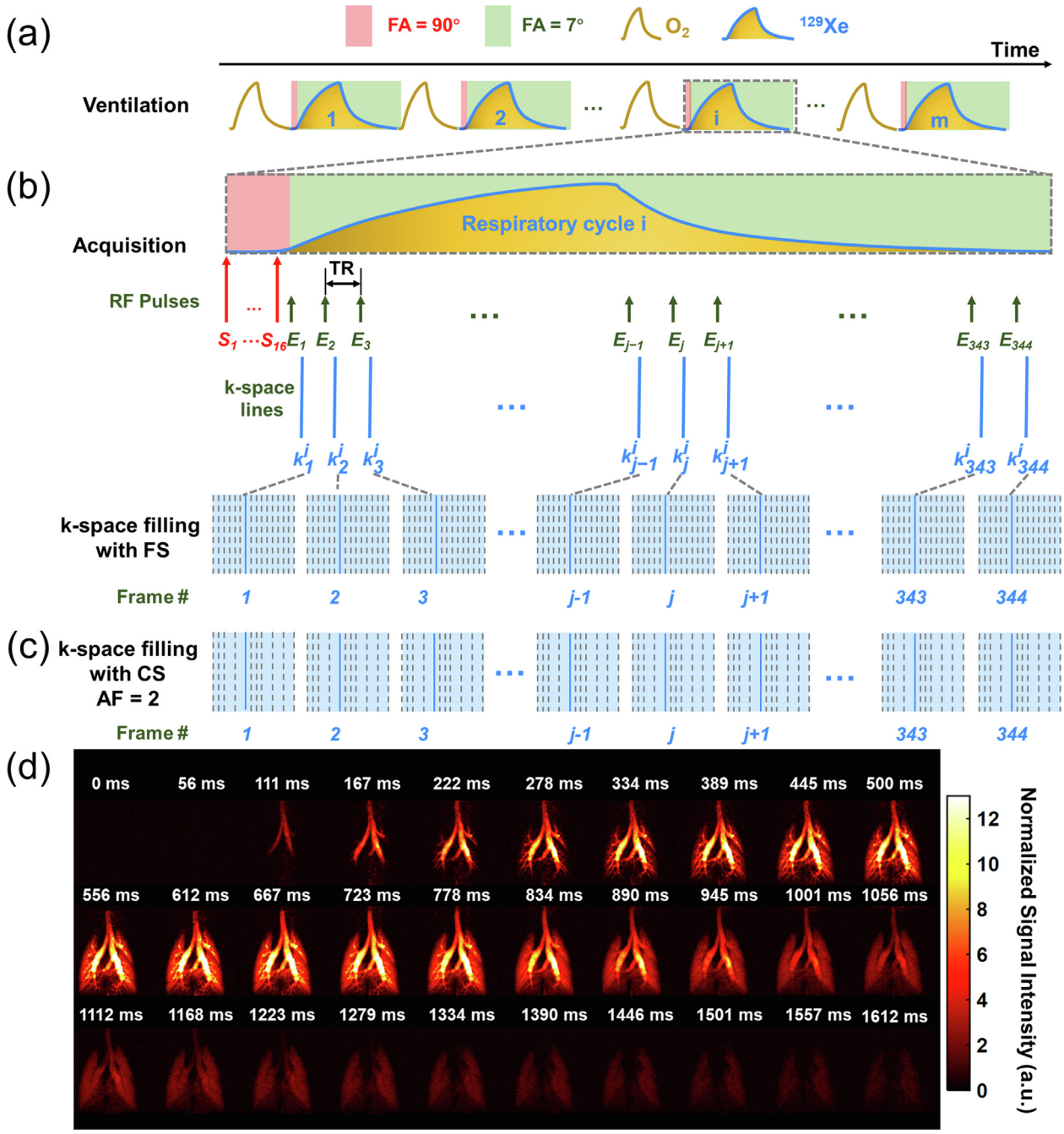

Fig. 1. Schematic of the ventilation, acquisition, and k-space lines filling strategies for dynamic ventilation imaging. (a) Ventilation strategy: to maintain normal physiological conditions and a stable detectable signal, oxygen, and xenon gas were alternatively ventilated into the lungs. The number below the blue curve indicates the ordinal number of ^{129}Xe breaths, and the number of ^{129}Xe breaths (m) corresponds to the number of phase encoding steps. (b) Acquisition and k-space filling strategies: to achieve high temporal resolution, k-space lines corresponding to the same phase encoding step of all the frame images were acquired in the same respiratory cycles, using a flip angle (FA) of 7°. Before MRI data acquisition in each respiratory cycle, sixteen saturation radio frequency (RF) pulses with a flip angle (FA) of 90° were applied (red arrows) to eliminate residual magnetization. For fully sampled k-space (FS), data collected during a single breathing cycle filled one line of each k-space. (c) k-space filling with compressed sensing (CS). To reduce acquisition time, a CS technique with an acceleration factor of 2 was employed, resulting in the acquisition of a total of 344 frame images. (d) Typical coronal dynamic ventilation images from a healthy rat. S denotes the saturation RF pulse, E denotes the excitation RF pulse, k_j represents the k-space number for the j^{th} frame image, and k_j^i indicates the i^{th} k space line in the j^{th} frame image.

compressed sensing technique was employed to accelerate image acquisition (Fig. 1c). Both retrospective and prospective results are provided in the supplementary materials (Fig. S1 online). All animal protocols were approved by the institutional animal care and use committee of the Innovation Academy for Precision Measurement Science and Technology, Chinese Academy of Sciences (APM22033A).

Using the proposed method, we successfully acquired dynamic ventilation images in rats with a temporal resolution of 5.6 ms and a nominal spatial resolution of 0.5 mm × 0.5 mm (Fig. 1d). Gas flow through the main trachea and bronchi and subsequently into the peripheral parenchyma during inspiration was clearly visualized, followed by a decrease in the ^{129}Xe signal during expiration, observed in the representative frames of the dynamic ventilation

(Fig. 1d) (the full series of dynamic images is presented in Fig. S2 online). To quantify gas flow within the lung, five representative regions of interest (ROI) were manually selected for quantitative analysis (Fig. S3a online). ^{129}Xe signals were successfully captured in all the five selected ROIs, with ^{129}Xe signal intensities in the trachea and bronchi being notably higher than those in the lung parenchyma. As expected, the ^{129}Xe signal dynamics closely followed the respiratory cycle, exhibiting a rapid increase during inspiration and a gradual decrease during expiration (Fig. S3b online). Additionally, we observe that the ^{129}Xe signal intensity in dynamic images captured during expiration was markedly lower than that acquired during inspiration. This reduction is likely attributable to the decay of HP gas magnetization caused by repeated RF excitations, combined with the absence of fresh HP gas supply during the expiration.

After confirming that the proposed method could be used for pulmonary dynamic ventilation imaging in healthy rats, we further evaluated its feasibility for assessing ventilation dysfunction associated with pulmonary diseases. Rats were treated with lipopolysaccharide (LPS), resulting in evident alveolar septal thickening and lung tissue consolidation (Fig. S4 online), thereby confirming the successful establishment of the pulmonary pathological animal model. Dynamic ventilation imaging was then performed in the diseased rats using the proposed method, and their ventilation performance was compared to that of healthy controls based on quantitative analysis of the recorded images. To facilitate image interpretation, we segmented the whole lung (WL) into four ROIs manually, as shown in Fig. 2a, i.e., the main trachea (ROI-T), left lobe (ROI-L), right upper lobe (ROI-RU), and right lower lobe (ROI-RL). The average signal intensities over time were then plotted for each ROI. The results revealed significantly lower dynamic ventilation signals ($P < 0.001$) in all three ROIs and WL in the LPS group compared to the healthy control group (Fig. 2b, d–f). Because the xenon gas was mechanically ventilated through a tube connected to the trachea at a constant flow rate (3.6 ml/s), no significant difference ($P = 0.208$) in ^{129}Xe signal intensity was observed in ROI-T between the groups. To minimize lung injury associated with mechanical ventilation, the pressure of the lung was maintained below 15 cm H_2O in all the rats throughout the experiments [13,14].

Additionally, total ^{129}Xe MR signal–time curves were calculated for each voxel using the registered dynamic images (Fig. 2g), from which gas volume–time curves were subsequently derived (Fig. 2h). Moreover, the maps of characteristic times related to

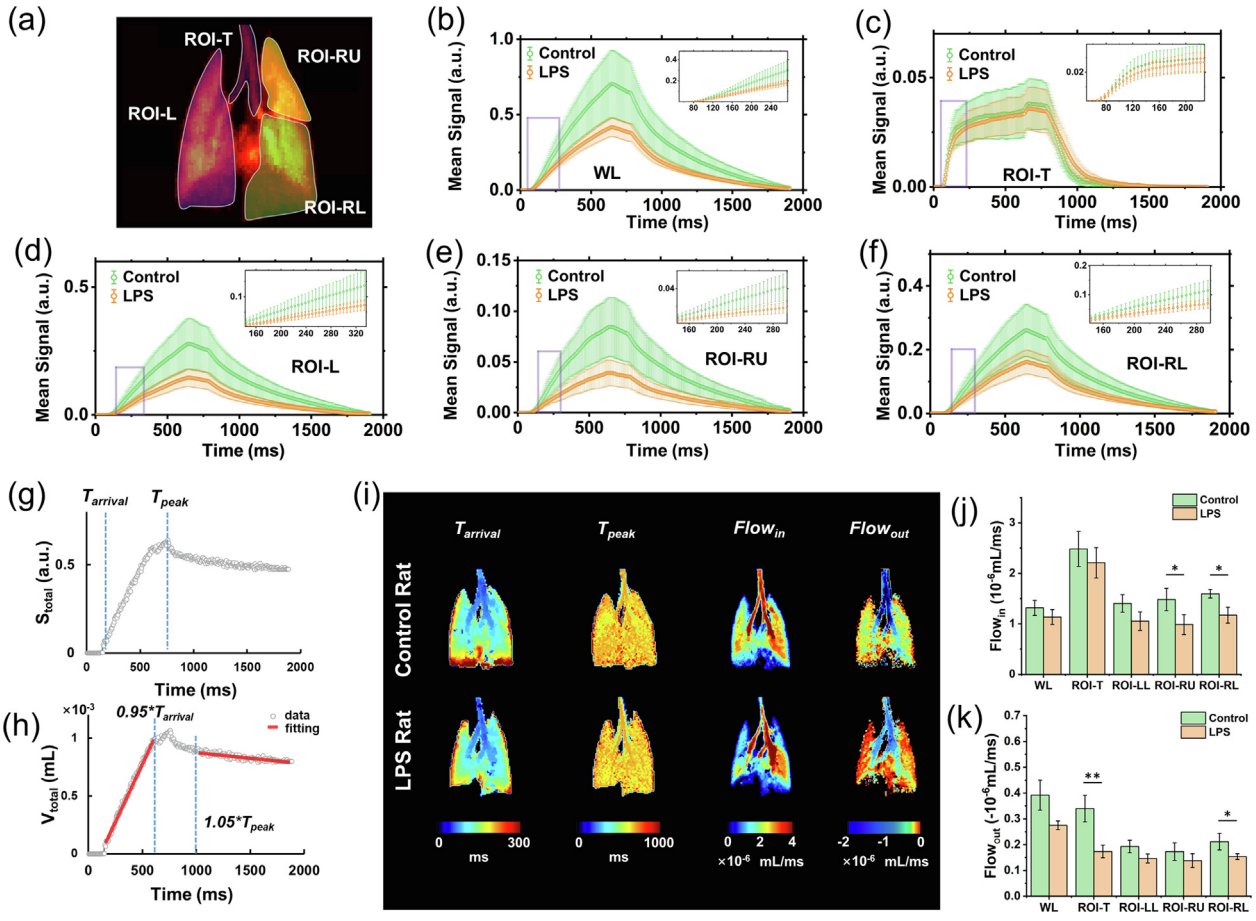

Fig. 2. Quantitative analysis of dynamic ventilation function based on signal-to-time curves and typical characteristic time and gas flow rate maps. (a) Lung images were manually segmented into four regions of interests (ROIs): the main trachea (ROI-T), left lobe (ROI-L), right upper lobe (ROI-RU), and right lower lobe (ROI-RL). Signal-to-time curves were generated for the whole lung (WL) (b), ROI-T (c), ROI-RU (d), ROI-L (e), and ROI-RL. (f) Comparison between LPS ($n = 5$) and control group ($n = 5$). Each figure includes a zoomed-in inset (highlighted by a purple box) providing a detailed view of a portion of the curves. A typical total ^{129}Xe signal–time curve (g) and ^{129}Xe gas volume–time curve (h) were obtained from a control rat. The time of gas arrival ($T_{arrival}$) and the time at which the signal reaches its peak (T_{peak}) is indicated, with fitted curves plotted in red. (i) Representative $T_{arrival}$ and T_{peak} maps, as well as gas flow rate for inspiration ($Flow_{in}$) and expiration ($Flow_{out}$), are presented for both control and LPS rats. Comparison of the averaged $Flow_{in}$ (j) and (k) values in the WL and four selected ROIs between the control ($n = 5$) and LPS ($n = 5$) groups. Comparison between groups was performed using a two-tailed Student's t-test or Mann-Whitney U test, with significance set at <0.05. Measures of central tendency are presented as the mean; error bars represent mean ± sd. All dynamic images were individually normalized to the maximum signal value of the entire respiratory cycle for each rat. Note: for display purposes, the $Flow_{out}$ values for ROI-T were multiplied by 0.2. $^{*}P < 0.05$, $^{**}P < 0.01$.

dynamic ventilation function were generated, including the time of gas arrival ($T_{arrival}$) and the time to peak signal intensity (T_{peak}), based on the total-signal-to-time curves for each rat [2]. Gas flow rate maps for inspiration ($Flow_{in}$) and expiration ($Flow_{out}$) were also created by applying linear fitting to the gas volume–time curves data on a voxel scale. The calculation methods are described in the supplementary materials online. Representative maps of characteristics times and gas flow rates from the control and LPS groups are shown in Fig. 2i. No significant differences were observed between the groups in the WL averaged parameters of $T_{arrival}$ (P_{adj} = 1.000) and T_{peak} (P_{adj} = 1.000), where P_{adj} denotes the Bonferroni corrected P value ($P_{adj} = P^*5$). However, compared to the control group, the LPS group exhibited greater heterogeneity in the $Flow_{in}$ and $Flow_{out}$ maps across the lung, and the measured global $Flow_{out}$ was significantly lower in the LPS group. Additionally, significant differences were observed in the measured regional $Flow_{in}$ (ROI-RU, P_{adj} = 0.045; ROI-RL, P_{adj} = 0.010) and $Flow_{out}$ (ROI-T, P_{adj} = 0.002; ROI-RL, P_{adj} = 0.045) between the groups (Fig. 2j and 2k). The measured characteristic times related to dynamic ventilation function for all the rats are summarized in Table S1 online, and the WL and regional $Flow_{in}$ and $Flow_{out}$ values are summarized in Table S2 online. The measured $Flow_{out}$ values are approximately 4–5 times lower than the $Flow_{in}$ values. This discrepancy is likely due to the difference in the concentration of "fresh HP ^{129}Xe" between inspiration and expiration. During inspiration, pure HP xenon gas is inhaled, whereas, during expiration, the exhaled gas contains a mixture of depolarized xenon and oxygen. Because the MRI signal is generated solely by HP ^{129}Xe, the measured $Flow_{out}$ values are significantly underestimated. To obtain more accurate $Flow_{out}$ values, it is essential to account for the proportion of HP ^{129}Xe in the exhaled gas. Without this correction, $Flow_{in}$ remains more sensitive to the dynamic changes in ventilation function compared to $Flow_{out}$, due to the higher SNR of images acquired during inspiration. Furthermore, both $Flow_{in}$ and $Flow_{out}$ demonstrated a correlation with histological measurements of alveolar septal thickness, as shown in Fig. S6 (online).

In conclusion, we developed an accelerated line-scan approach for pulmonary dynamic ventilation function imaging, achieving substantial improvements in both temporal and spatial resolution up to several milliseconds and submillimeter levels, respectively. Several key parameters derived from the quantitative analysis of the images are proposed and successfully applied for the regional dynamic ventilation abnormalities assessment *in vivo*. Although clinical translation presents challenges—particularly in achieving stable and reproducible gas delivery in human lungs—the prior validation of multiple-breath ^{129}Xe gas imaging in human studies supports its feasibility for clinical implementation [15]. These findings have the potential to provide new insights into the understanding and early diagnosis of lung diseases associated with dynamic ventilation dysfunction.

Conflict of interest

The authors declare that they have no conflict of interest.

Acknowledgments

This work was supported by the National key Research and Development Program of China (2023YFF0722200), the National Natural Science Foundation of China (82127802, 82372150, 82441015, and 82202119), the Strategic Priority Research Program of the Chinese Academy of Sciences (XDC0170000 and XDB0540000), Key Research Program of Frontier Sciences, CAS (ZDBS-LY-JSC004), Hubei Provincial Key Technology Foundation of China (2021ACA013), Major Program (JD) of Hubei Province (2023BAA021) and Hubei Province Outstanding Youth Fund (2023AFA112, 2022CFA050). Haidong Li and Xiuchao Zhao acknowledge the support from the Youth Innovation Promotion Association, CAS (2020330, 2021330). The authors would like to thank Prof. Daiqin Chen for polishing the manuscript.

Author contributions

Haidong Li and Xin Zhou designed research. Hongchuang Li, Haidong Li, Li Fan, Xiaoling Liu, and Yeqing Han performed research. Hongchuang Li, Haidong Li, Li Fan, Ming Zhang, and Xiuchao Zhao analyzed data. and Hongchuang Li, Haidong Li, Yang Jin, Louis-S. Bouchard, Shiyuan Liu, and Xin Zhou wrote the paper.

Appendix A. Supplementary material

Supplementary data to this article can be found online at https://doi.org/10.1016/j.scib.2025.05.014.

References

[1] Hogg JC, McDonough JE, Suzuki M. Small airway obstruction in COPD: new insights based on micro-CT imaging and MRI imaging. Chest 2013;143:1436–43.
[2] Koumellis P, van Beek EJ, Woodhouse N, et al. Quantitative analysis of regional airways obstruction using dynamic hyperpolarized ^{3}He MRI-preliminary results in children with cystic fibrosis. J Magn Reson Imaging 2005;22:420–6.
[3] de Lange EE, Altes TA, Patrie JT, et al. Evaluation of asthma with hyperpolarized helium-3 MRI: correlation with clinical severity and spirometry. Chest 2006;130:1055–62.
[4] Guerrero T, Sanders K, Castillo E, et al. Dynamic ventilation imaging from four-dimensional computed tomography. Phys Med Biol 2006;51:777–91.
[5] Kaireit TF, Kern A, Voskrebenzev A, et al. Flow volume loop and regional ventilation assessment using phase-resolved functional lung (PREFUL) MRI: comparison with ^{129}Xenon ventilation MRI and lung function testing. J Magn Reson Imaging 2021;53:1092–105.
[6] Rao Q, Li H, Zhou Q, et al. Assessment of pulmonary physiological changes caused by aging, cigarette smoking, and COPD with hyperpolarized ^{129}Xe magnetic resonance. Eur Radiol 2024;34:7450–9.
[7] Li H, Li H, Zhang M, et al. Direct imaging of pulmonary gas exchange with hyperpolarized xenon MRI. Innovation 2024;5:100720.
[8] Chen M, Doganay O, Matin T, et al. Delayed ventilation assessment using fast dynamic hyperpolarised Xenon-129 magnetic resonance imaging. Eur Radiol 2020;30:1145–55.
[9] Kyriazis A, Rodriguez I, Nin N, et al. Dynamic ventilation ^{3}He MRI for the quantification of disease in the rat lung. IEEE Trans Biomed Eng 2012;59:777–86.
[10] Collier GJ, Wild JM. *In vivo* measurement of gas flow in human airways with hyperpolarized gas MRI and compressed sensing. Magn Reson Med 2015;73:2255–61.
[11] Xiao S, Deng H, Duan C, et al. Highly and adaptively undersampling pattern for pulmonary hyperpolarized ^{129}Xe dynamic MRI. IEEE Trans Med Imaging 2019;38:1240–50.
[12] Raimondo L, Knapen T, Oliveira ŁAF, et al. A line through the brain: implementation of human line-scanning at 7T for ultra-high spatiotemporal resolution fMRI. J Cereb Blood Flow Metab 2021;41:2831–43.
[13] Freeman MS, Cleveland ZI, Qi Y, et al. Enabling hyperpolarized ^{129}Xe MR spectroscopy and imaging of pulmonary gas transfer to the red blood cells in transgenic mice expressing human hemoglobin. Magn Reson Med 2013;70:1192–9.
[14] Virgincar RS, Dahlke J, Robertson SH, et al. A portable ventilator with integrated physiologic monitoring for hyperpolarized ^{129}Xe MRI in rodents. J Magn Reson 2018;295:63–71.
[15] Hamedani H, Clapp JT, Kadlecek SJ, et al. Regional fractional ventilation by using multibreath wash-in ^{3}He MR imaging. Radiology 2016;279:917–24.